www.acsmaterialsletters.org

Metallic Conductivity of $Ti_3C_2T_x$ MXene Confirmed by Temperature-Dependent **Electrical Measurements**

Alexey Lipatov,* Saman Bagheri, and Alexander Sinitskii*



Downloaded via UNIV OF NEBRASKA LINCOLN on March 20, 2024 at 19:53:26 (UTC). See https://pubs.acs.org/sharingguidelines for options on how to legitimately share published articles.

Cite This: ACS Materials Lett. 2024, 6, 298-307



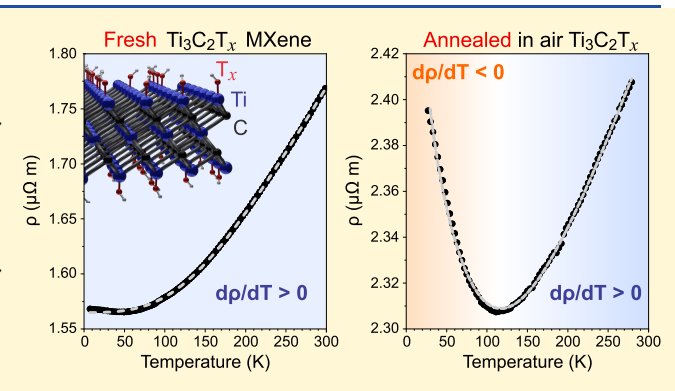
ACCESS

Metrics & More

Article Recommendations

Supporting Information

ABSTRACT: Ti₃C₂T_x, the most popular MXene to date, is widely regarded as a metallic material, based on numerous theoretical predictions and the results of experimental studies. Yet, despite this general consensus on the metallic nature of Ti₃C₂T_x, there have not been reports on its temperaturedependent resistivity (ρ) measurements that would demonstrate the expected increase of resistivity with temperature with $d\rho/dT$ > 0 in a wide temperature range. Instead, all $\rho(T)$ data reported so far, which were mostly collected on macroscopic films of percolating Ti₃C₂T_x flakes, demonstrate dependences with minima, which were observed in the range from 90 to 250 K in different measurements. In this study, we fabricated electronic devices based on individual high-quality Ti₃C₂T_x



flakes and performed their temperature-dependent resistivity measurements. The resistivity of flakes was found to increase with temperature in the 10-300 K range, and the resulting $\rho(T)$ dependences can be accurately described by the Bloch-Grüneisen model for the temperature dependence of the resistivity of metals, confirming the metallic nature of Ti₃C₂T_x. We also demonstrate that an oxidation of a $Ti_3C_2T_x$ monolayer transforms a monotonically increasing $\rho(T)$ curve into a dependence with a minimum that looks similar to the previously reported results for percolating MXene films. The emerging low-temperature tail with a semiconductor-like $d\rho/dT < 0$ behavior can be explained by the stronger electron scattering in a partially oxidized MXene due to an increased level of disorder, and the resulting $\rho(T)$ curves can be accurately fitted using Matthiessen's rule, which incorporates the effect of all types of scatterers on the transport properties of metals. These experiments verify the metallic nature of $Ti_3C_2T_x$ ($d\rho/dT > 0$) and provide insights into the origin of the emergence of a lowtemperature tail with $d\rho/dT < 0$. We also demonstrate that multilayer $Ti_3C_2T_x$ flakes retain their purely metallic $d\rho/dT > 0$ behavior even after annealing in air, suggesting that the outer layers of multilayer flakes effectively protect the core layers from oxidation. This result suggests that certain applications may benefit from the use of multilayer flakes because of their improved environmental stability.

Xenes are a rapidly growing family of twodimensional (2D) transition metal carbides, nitrides, and carbonitrides with a general formula of $M_{n+1}X_nT_x$, where M is a transition metal, such as Ti, Nb, V, Cr, etc., X is carbon and/or nitrogen, n = 1, 2, 3, 4, or 5, and T_x represents the surface functional groups. 1,2 More than 30 different MXenes have been demonstrated experimentally, and many others have been predicted theoretically. MXenes are finding numerous applications in many different areas ranging from energy storage and electromagnetic interference shielding to gas sensing and nanoelectromechanical systems. 1,2 Many of these applications rely on the high electrical conductivities of some of the MXene materials. In particular, Ti₃C₂T_x, which is the most popular MXene material to date, is known for its

very high electrical conductivity of up to 11000 S cm⁻¹, which was measured on individual monolayer flakes.3 Yet, despite the great interest in electronic applications of Ti₃C₂T_x, many aspects of its electronic properties require further investigation. In particular, while this MXene is widely discussed as a metallic material in both theoretical^{4,5} and experimental studies,^{6–9} the reported temperature dependences of the resistivity (ρ) for

Received: October 11, 2023 Revised: December 11, 2023 Accepted: December 11, 2023 Published: December 19, 2023





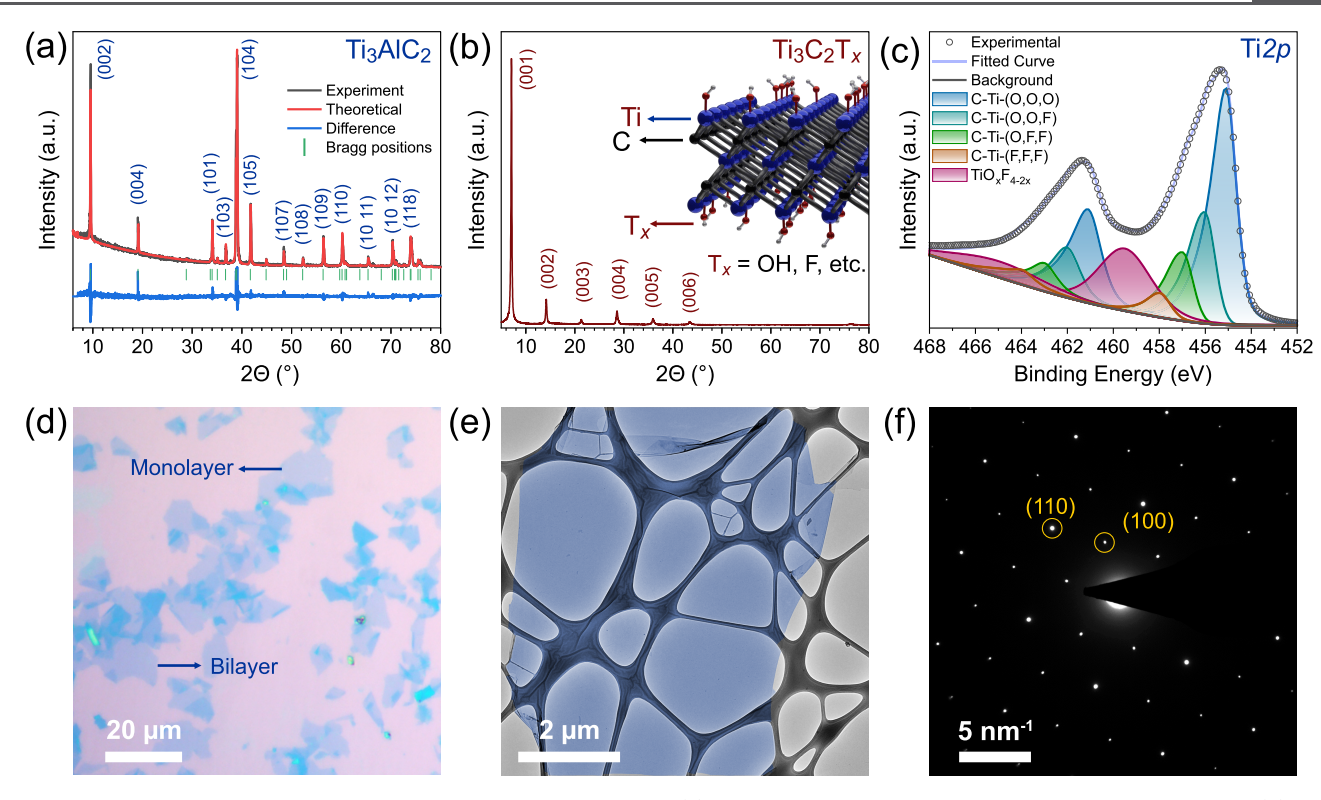


Figure 1. Characterization of Ti_3AlC_2 MAX phase and $Ti_3C_2T_x$ MXene. (a) XRD pattern of a Ti_3AlC_2 powder with Rietveld analysis. (b) XRD pattern of a $Ti_3C_2T_x$ film. The inset shows a fragment of the structure of a $Ti_3C_2T_x$ monolayer. (c) High-resolution XPS Ti2p spectrum of $Ti_3C_2T_x$ and its analysis. (d) Optical microscopy image of $Ti_3C_2T_x$ flakes on a Si/SiO_2 substrate. (e) False-color TEM image of a $Ti_3C_2T_x$ flake on a lacey carbon grid. The $Ti_3C_2T_x$ flake is colored blue for clarity. (f) SAED image of the $Ti_3C_2T_x$ flake shown in panel (e).

 ${
m Ti}_3{
m C}_2{
m T}_x$ were not entirely consistent with its metallic character. ${}^{9-11}$ The $\rho(T)$ plots for ${
m Ti}_3{
m C}_2{
m T}_x$ reported in previous papers have variations from each other, although they can generally be described as dependences with a minimum. At low temperatures, the resistivity of ${
m Ti}_3{
m C}_2{
m T}_x$ MXene exhibited a semiconductor-like behavior with ${
m d}\rho/{
m d}T<0$, while at higher temperatures, it showed a metallic-like behavior with ${
m d}\rho/{
m d}T>0$. The slopes of the semiconductor- and metallic-like regions varied considerably for different measurements, and so did the temperature of the resistivity minimum, which was observed around 90 K, 9 140 K, 10 or 250 K. 11

Considering the immense importance of Ti₃C₂T_x as the most popular MXene material, it is necessary to identify the origin of these discrepancies and determine whether the metallic character of Ti₃C₂T_x could be inferred from its temperature-dependent electrical measurements. One possible factor contributing to the differences in the results of prior electrical measurements is the different nature of the investigated samples of MXenes, which were tested as thin films of Ti₃C₂T_x prepared by etching of sputter-deposited epitaxial Ti₃AlC₂, filtered films of solution-synthesized flakes, 10 or individual Ti₃C₂T_x flakes. 11 For an investigation of the intrinsic properties of MXenes, it is preferable to perform single-flake measurements, as multiflake studies, for example, on bulk filtrates need to account for the effects of contact resistances between different flakes and the presence of the residual solvent molecules, etchants, and other adsorbate species that may be trapped between the flakes. Also, since $Ti_3C_2T_x$ MXene is known to be prone to oxidation, $^{12-14}$ a material degradation may affect the shape of the temperature dependence of the resistivity and introduce a semiconductorlike region in the otherwise metallic $\rho(T)$ curve. To test this

hypothesis, we prepared electronic devices based on individual Ti₃C₂T_x flakes, with a particular focus on minimizing their storage time in aqueous solution and exposure to ambient conditions during device fabrication. The devices were quickly fabricated right after the MXene synthesis and immediately loaded into a vacuum chamber of a probe station, where they were isolated from the environment. The vacuum-measured Ti₃C₂T_r MXene flakes with a minimal degree of oxidation exhibited a metallic-like behavior with $d\rho/dT > 0$ in the entire temperature range from 10 to 300 K. Then, to test the effect of oxidation on Ti₃C₂T_x, we annealed the devices in air and then remeasured them in the same conditions. Remarkably, after the annealing of the $Ti_3C_2T_x$ devices, we observed a different $\rho(T)$ dependence that was qualitatively similar to the previous reports, $^{9-11}$ with $d\rho/dT < 0$ at low temperatures and $d\rho/dT >$ 0 at high temperatures.

This study provides several insights into the electronic properties of Ti₃C₂T_x MXene. First, it demonstrates that freshly prepared and tested Ti₃C₂T_x MXene flakes exhibit the metallic-like temperature dependence of the resistivity with $d\rho/dT > 0$ in a broad temperature range. This observation confirms the widespread view of Ti₃C₂T_x MXene as a metallic material, 4-7,9 which previously was not entirely supported by the temperature-dependent electrical measurements. Second, this study shows that the electronic properties of Ti₃C₂T_x monolayers are sensitive to oxidation, suggesting that $\rho(T)$ measurements may be used for the assessment of the quality of MXene materials and their suitability for specific applications. For example, the electronic applications require pristine MXenes with the highest electrical conductivity,³ while other applications, such as gas sensing, may benefit from a partial oxidation of a material. 15-19 Finally, we demonstrate that

unlike their monolayer counterparts, the multilayer $Ti_3C_2T_x$ flakes retain their purely metallic $d\rho/dT>0$ behavior even after oxidation in air, suggesting that the outer layers of multilayer flakes effectively protect the core layers from the environment. While many studies focus on the optimization of exfoliation of MXene materials down to the monolayer limit, 20,21 the results of this work suggest that certain applications may benefit from the use of multilayer flakes because of their improved environmental stability.

To assess the intrinsic electronic properties of $Ti_3C_2T_x$, it was important to ensure that the MXene flakes used for device fabrication were of the highest quality possible with the currently available synthetic approaches. Over the past decade there has been a strong effort to optimize the synthesis of $Ti_3C_2T_{xy}$ which resulted in the notable improvement of the quality of MXene flakes in terms of their size, uniformity, and the amount of defects and impurities.²⁰ Synthesis of highquality Ti₃C₂T_x MXene starts with the optimized synthesis of the precursor Ti_3AlC_2 MAX phase. ²² Commonly, Ti_3AlC_2 can be prepared from either a mixture of elemental precursors, Ti, Al, and C, taken at a 3:1.1:2 stoichiometric ratio, or a mixture of TiC, Al, and Ti taken at a 2:1.1:1 stoichiometric ratio.²³ Mathis and co-workers have recently demonstrated that increasing the content of Al in the precursor mixture to TiC:Al:Ti = 2:2:1 improves the overall quality of the MAX phase.²² The resulting MAX phase has fewer defects, leading to the formation of MXenes with superior resistance to oxidation compared to the previously synthesized Ti₃C₂T_x. Accordingly, we used this modified synthetic approach to produce Ti₃AlC₂ from a mixture of TiC, Al, and Ti (2:2:1).²² The resulting MAX phase was characterized by powder X-ray diffraction (XRD), and the diffraction pattern was analyzed using the Rietveld method. The results are presented in Figure 1a, where all experimentally observed peaks are indexed and fitted with a theoretical pattern. The produced Ti₃AlC₂ MAX phase was highly crystalline, and no impurity phases were observed. After sieving and processing of the MAX phase, as described in the Experimental Section, we used the sieved fraction with particle sizes below 38 μ m to synthesize $Ti_3C_2T_x$; see Figure S1 in the Supporting Information.

MXene monolayers were prepared using the minimally intensive layer delamination (MILD) method, ¹³ which employs a mixture of LiF and HCl for the etching of Ti₃AlC₂. This etchant is less aggressive than concentrated HF, which removes Al from Ti₃AlC₂ faster but results in severe degradation of MXene flakes. ^{20,24} In contrast, the LiF-HCl mixture slowly generates HF *in situ*, and although the etching process takes a longer time compared to the direct use of concentrated HF, it results in a MXene material of higher quality. ^{13,20} After aluminum etching, the sample was washed with deionized (DI) water. Following the guidelines by Shekhirev et al., ²¹ we avoided any unnecessary agitation of the MXene suspension, which was shown to reduce the flake size. ¹³ Instead, the MXene particles were gently delaminated by a mild shaking of the suspension. ²⁵

Figure 1b shows an XRD pattern recorded on a vacuum-filtered film of $Ti_3C_2T_x$ MXene flakes. It confirms the conversion of Ti_3AlC_2 to $Ti_3C_2T_x$, as no peaks corresponding to the precursor MAX phase or other crystalline impurities were observed, and the only visible reflections are the series of (00l) peaks (l = 1, 2, 3, ...) originating from the layered structure of the stacked MXene flakes in a film.³ According to the XRD results, the interlayer spacing between the flakes in a

vacuum-filtered film was 1.247 nm $(2\theta_{001} = 7.08^\circ)$, which is larger than the nominal thickness of a ${\rm Ti_3C_2T_x}$ monolayer of 0.98 nm^{3,9,26,27} and suggests the presence of various intercalants, such as water molecules, trapped between the MXene sheets in their bulk assemblies.

In order to demonstrate the high quality of the synthesized MXene material, we analyzed it using X-ray photoelectron spectroscopy (XPS). Figure 1c shows a high-resolution XPS Ti2p spectrum of Ti₃C₂T_x. The spectrum was analyzed using the Fit-V protocol described by Natu and co-workers, ²⁸ with the following $Ti2p_{3/2}$ fitting components: C-Ti-(O,O,O) at 455.1 eV, C-Ti-(O,O,F) at 456.0 eV, C-Ti-(O,F,F) at 456.9 eV, C-Ti-(F,F,F) at 457.8 eV, and TiO_{2-x}F_{2x} at 459.5 eV. For the oxidized $Ti_3C_2T_x$ materials, the latter component is often observed as a well-developed peak,²⁸ so the fact that in this spectrum (Figure 1c) it is only discernible in the fitting suggests a mild degree of oxidation in the as-synthesized MXene material. The overall shape of the XPS Ti2p spectrum in Figure 1c is comparable to such spectra of other MXene materials reported in the studies focused on the optimization of the synthesis of ${\rm Ti}_3{\rm C}_2{\rm T}_x$. The XPS survey and highresolution Al2p spectra are shown in Figure S2 in the Supporting Information and confirm the complete removal of Al during the etching of Ti₂AlC₂, as well as the presence of Ti, C, F, and O in the MXene material.

Figure 1d demonstrates an optical microscopy image of MXene flakes deposited on a Si/SiO $_2$ substrate; additional images are provided in Figure S3 in the Supporting Information. Since any unnecessary agitation of the MXene suspension was avoided, following the guidelines by Shekhirev et al., 21 the flakes were visually uniform and large, mostly in the 15–20 μ m range, facilitating the device fabrication. Furthermore, since the MXene suspension was minimally disturbed, the exfoliation of the etched MXene particles down to the monolayer limit was not complete, and in addition to the monolayer flakes, multiple bilayer and multilayer flakes were also observed on the substrate (Figure S3). The presence of ${\rm Ti}_3{\rm C}_2{\rm T}_x$ with different thicknesses was beneficial for this study, as both monolayer and multilayer flakes were used for device fabrication and electrical measurements.

The transmission electron microscopy (TEM) image of a representative ${\rm Ti_3C_2T_x}$ flake (Figure 1e) shows that the MXene surface looked clean, and no pinholes or ${\rm TiO_2}$ nanoparticles were observed, which, if present, would indicate degradation of ${\rm Ti_3C_2T_x}^{12,15,19}$ The selected-area electron diffraction (SAED) pattern of the same flake (Figure 1f) demonstrates its high crystallinity and phase purity. The observed diffraction spots demonstrate the hexagonal arrangement of the atoms in the MXene sheet. No diffraction spots corresponding to any phases other than ${\rm Ti_3C_2T_x}$, such as ${\rm TiO_2}$, ${}^{\rm 12,15}$ were observed. Overall, the materials characterization results presented in Figure 1 indicate that the synthesized ${\rm Ti_3C_2T_x}$ was of high quality, comparable to the best MXene samples reported in the literature to date.

After the synthesis, the as-prepared ${\rm Ti_3C_2T_x}$ was immediately used for the device fabrication. During the cleanroom work, the flakes deposited on a ${\rm Si/SiO_2}$ substrate were mostly isolated from the environment while being in the vacuum chambers of either an electron-beam lithography (EBL) writer or an electron-beam evaporator. After the completion of the cleanroom work, the devices were immediately loaded into the vacuum chamber of a cryogenic probe station, where they were kept at a pressure of about 2×10^{-6} Torr for electrical

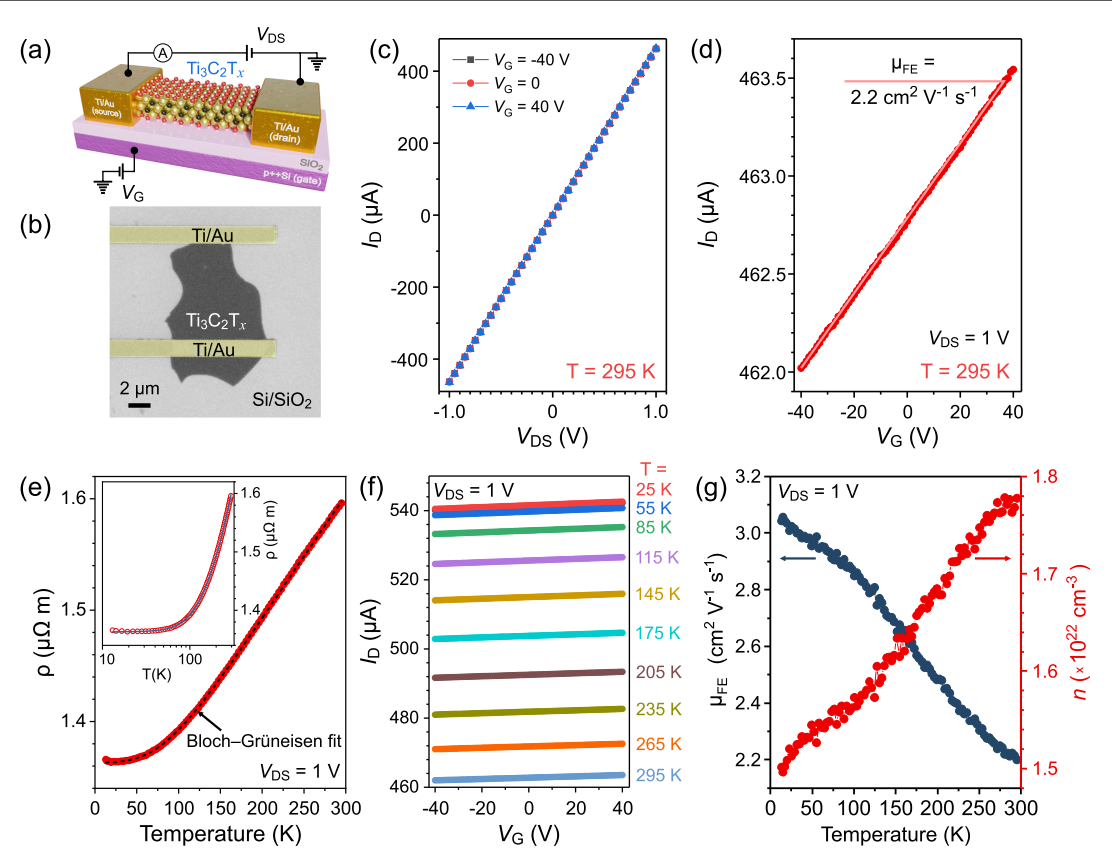


Figure 2. Electronic properties of a device based on an individual monolayer $Ti_3C_2T_x$ flake. (a) Scheme of FET with a $Ti_3C_2T_x$ channel. (b) False-color SEM image of a $Ti_3C_2T_x$ device. The Ti/Au electrodes are colored yellow for clarity. (c) Room-temperature I_D-V_{DS} curves at different gate voltages for the $Ti_3C_2T_x$ device shown in panel (b). (d) Room-temperature transfer characteristic of the same device measured at $V_{DS}=1$ V. The highlighted linear slope was used for calculating the field-effect mobility. (e) Temperature-dependent resistance (red dots) of the same monolayer $Ti_3C_2T_x$ device fitted using the Bloch-Grüneisen formula (dashed black curve). The inset demonstrates the same dependence with temperature shown on a semilogarithmic scale. (f) Transfer characteristics of the same device at different temperatures. (g) Field-effect mobility and charge carrier concentration of the same $Ti_3C_2T_x$ device at different temperatures.

measurements. As a result, the total time of exposure of $Ti_3C_2T_x$ flakes to air was less than 1 h.

The scheme of the MXene-based two-terminal field-effect transistor (FET) devices fabricated in this work by EBL is shown in Figure 2a. A MXene flake is bridging source (S) and drain (D) electrodes that were prepared by depositing 5 nm of Ti and 15 nm of Au. The devices were fabricated on a p-doped Si substrate covered with a 300-nm-thick SiO₂ layer; the p⁺⁺-Si was used as a gate (G) electrode in electrical measurements. Figure 2b shows a scanning electron microscopy (SEM) image of a representative device based on a monolayer Ti₂C₂T_x flake. The lateral dimensions of this flake are 8.8 μ m (distance between electrodes) and 6.6 μ m (average width of the flake). The monolayer character of the flake was confirmed by atomic force microscopy (AFM), which revealed a thickness of about 2.7 nm, consistent with the previous results of AFM measurements of Ti₃C₂T_x monolayers on Si/SiO₂ substrates.^{3,13,26} This thickness is larger than the theoretical thickness of a Ti₃C₂T_x monolayer of about 0.98 nm, ^{3,9,26,27} likely due to the presence of adsorbed molecules, such as water, on and under the flakes measured in ambient conditions. The AFM of the device was performed after its electrical characterization. For the resistivity calculations, we used the nominal thickness of monolayer Ti₃C₂T_x.

Figure 2c,d summarizes the results of room-temperature electrical measurements of the MXene device shown in Figure 2b. Figure 2c shows the dependence of the drain current $(I_{\rm D})$

on the drain-source voltage $(V_{\rm DS})$ at the gate voltages $(V_{\rm G})$ of -40, 0, and 40 V applied to the bottom electrode. The field effect is weak, as the three $I_{\mathrm{D}}{-}V_{\mathrm{DS}}$ dependences nearly coincide. In the $V_{\rm DS}$ range from -1 to 1 V, the $I_{\rm D}-V_{\rm DS}$ curves show linear dependence at all studied V_G values, suggesting good electrical contacts between the Ti/Au electrodes and the MXene channel. The room-temperature resistance of this device is 2160 Ω . Sheet resistance (ρ_{\blacksquare}) values for the devices were calculated from the $I_{\rm D}{-}V_{\rm DS}$ dependences measured at $V_{\rm G}$ = 0 using the flake dimensions. For the device shown in Figure 2, $\rho_{\blacksquare} = 1630 \ \Omega \ \Box^{-1}$. The MXene resistivity (ρ) can be estimated by multiplying the sheet resistance by the thickness of a MXene monolayer of 0.98 nm, 3,9,26,27 yielding 1.60 $\mu\Omega$ m. This value corresponds to the conductivity (σ) of 6260 S cm⁻¹, which is comparable to our previous results of electrical measurements on high-quality $\tilde{{\rm Ti}}_{3}{\rm C}_{2}{\rm T}_{x}$ monolayers. 3,13,21 The $I_{\rm D} - V_{\rm G}$ plot for the same device at $V_{\rm DS}$ = 1 V is presented in Figure 2d, showing a linear dependence with a positive slope, suggesting n-type transport. The field-effect mobility (μ_{FE}) was extracted from this I_D - V_G dependence using the formula

$$\mu_{\rm FE} = \frac{1}{C_d} \times \frac{\delta(1/\rho_{\blacksquare})}{\delta V_{\rm G}} \tag{1}$$

where C_d is the capacitance of a 300-nm-thick SiO₂ dielectric layer. The $\mu_{\rm FE}$ for the presented device was calculated to be about 2.2 cm² V⁻¹ s⁻¹, which is also comparable to the results

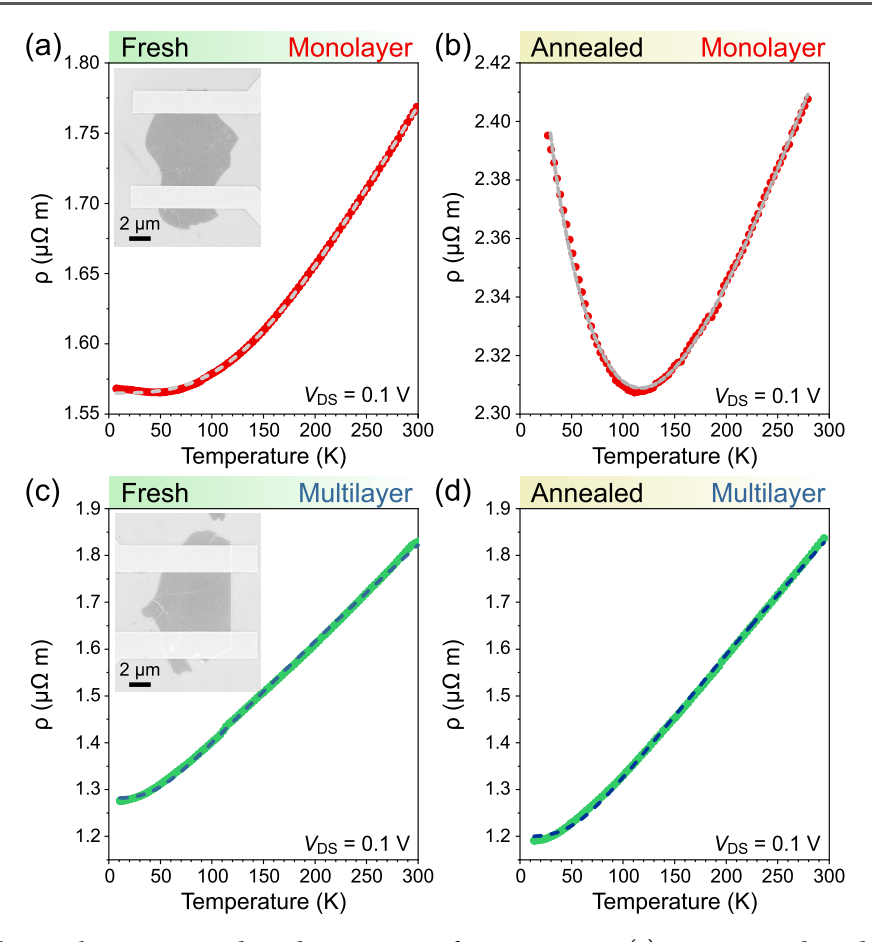


Figure 3. Effect of annealing on the temperature-dependent resistivity of $Ti_3C_2T_x$ MXene. (a) Temperature-dependent resistivity of a freshly fabricated monolayer $Ti_3C_2T_x$ device, fitted with eq 2. The inset shows the SEM image of the device. (b) Temperature-dependent resistivity of the same device as in (a) after annealing in air (see the main text for details), fitted with eq 3. (c) Temperature-dependent resistivity of a freshly fabricated multilayer $Ti_3C_2T_x$ device, fitted with eq 2. The inset shows the SEM image of the device. (d) Temperature-dependent resistivity of the same device as in (c) after annealing in air, fitted with eq 2. All measurements were performed at $V_{DS} = 0.1$ V.

of our previous studies. 3,13,21 The transfer characteristic of the MXene device has low noise (Figure 2d), which is another indicator of good sample quality. Based on the measured conductivity and mobility values, this monolayer flake has a charge carrier concentration of $n \approx 1.8 \times 10^{22}$ cm⁻³, which is comparable to other reports on electrical measurements of $\text{Ti}_3\text{C}_2\text{T}_x$ MXene. 11,30

We then studied the electronic properties of MXene devices in the temperature range from 9 to 300 K. The measurements were performed in 3 K steps with 15 min of temperature stabilization between the steps. For the same monolayer $Ti_3C_2T_x$ device (Figure 2b), the temperature dependence of resistivity shown in Figure 2e demonstrates $d\rho/dT > 0$ in the entire measurement temperature range, in remarkable difference with the results presented in prior literature. 9-11 As the temperature decreases from 300 K to approximately 100 K, the resistance of the Ti₃C₂T_x monolayer decreases linearly. The slope of the $\rho(T)$ dependence slowly decreases at lower temperatures, and the resistivity reaches the residual value of about 1.36 $\mu\Omega$ m. The residual resistivity is a result of the electron scattering on static defects that disturb the periodicity of the lattice, such as grain boundaries, impurities, and surfaces.³¹ The surface contribution should be especially pronounced because of the 2D nature of the material and the fact that the MXene terminal groups are disordered. 32,33

The inset in Figure 2e shows the same plot but with a logarithmic temperature scale.

The dependence shown in Figure 2e is a classic example of the temperature dependence of the resistivity of metals and can be described using the Bloch–Grüneisen model, which is applicable to 2D materials: ^{34,35}

$$\rho(T) = \rho_0 + \rho_0 A \left(\frac{T}{\theta_{BG}}\right)^n \int_0^{\theta_{BG}/T} \frac{x^n}{(e^x - 1)(1 - e^{-x})} dx$$
(2)

where ρ_0 is the residual resistivity, A is a constant related to electron—phonon scattering, $\Theta_{\rm BG}$ is the Bloch—Grüneisen temperature, and n=3 for the case of s-d electron scattering in transition metals, 36 as in ${\rm Ti}_3{\rm C}_2{\rm T}_x$ MXene. The formula allows extraction of the Bloch—Grüneisen temperature, which was found to be $\Theta_{\rm BG}=657$ K for a monolayer flake. The excellent fitting ($R^2=0.99993$) shown as a dashed black curve in Figure 2e suggests the validity of this model and indicates that the electron—phonon scattering dominates the temperature-dependent part of the electrical resistivity.

Changes in electron mobility of the ${\rm Ti_3C_2T_x}$ MXene monolayer with temperature were revealed through analysis of the transfer characteristics, i.e., the $I_{\rm D}$ – $V_{\rm G}$ dependences, measured at different temperatures. The transfer characteristics of the monolayer MXene device at selected temperatures are presented in Figure 2f. All curves are qualitatively similar,

showing linear dependences on gate voltage and positive slopes, consistent with n-type behavior. From these transfer characteristics, we can extract $\mu_{\rm FE}$ values at different temperatures using eq 1. The resulting temperature dependence of $\mu_{\rm FE}$ is shown in Figure 2g. The field-effect mobility increases as the temperature decreases, from 2.2 cm² V $^{-1}$ s $^{-1}$ at 300 K to 3.0 cm² V $^{-1}$ s $^{-1}$ at 13 K. This observation is consistent with the behavior of electrons in metals, in which the conductivity increase at lower temperatures is caused by a reduced electron scattering due to the suppressed phonons, resulting in an increase of the electron mean free path. In contrast, the charge carrier concentration shows little dependence on temperature, as demonstrated in Figure 2g. As the temperature decreases from 300 to 13 K, the n values decrease from 1.8×10^{22} to 1.5×10^{22} cm $^{-3}$.

It is well established that most MXenes contain a certain amount of oxygen species, which can be present as surface functional groups, 6,32 oxygen atoms incorporated in the carbon sublattice, 37 or both. The as-prepared Ti₃C₂T_x samples synthesized by the standard solution etching procedures²⁰ involving highly acidic conditions already contain oxygen, as shown by numerous XPS studies.²⁸ The Ti₃C₂T_x flakes that are exposed to ambient conditions further oxidize with time, ¹³ and the degradation process is greatly accelerated if a MXene material is annealed in air. 15 Therefore, considering that all solution-synthesized $Ti_3C_2T_x$ materials are oxidized to a certain extent, we decided to investigate how the degree of oxidation of the flakes affects their temperature-dependent resistivity behavior. For this experiment, we started with freshly prepared Ti₃C₂T_r flakes with a minimal degree of oxidation that is currently achievable with the presently available synthetic approaches^{20,22} (Figure 1) and then intentionally oxidized them by a mild annealing in air, comparing the electrical properties of the same flakes before and after oxidation.

We first investigated the effect of oxidation on the electrical properties of the monolayer Ti₃C₂T_x flakes. Figure 3a shows the temperature dependence of the resistivity of a freshly prepared monolayer $Ti_3C_2T_x$ flake that is shown in the SEM image in the inset. The room-temperature resistance of this device is 1804 Ω , which, accounting for the device dimensions, translates into $\rho_{\blacksquare} = 1800 \ \Omega \ \Box^{-1}$, $\rho = 1.77 \ \mu\Omega$ m, and $\sigma =$ 5660 S cm⁻¹. The temperature dependence of the resistivity shows metallic behavior (Figure 3a) and can be accurately fitted using eq 2. After the measurements, the device was heated on a hot plate in air at 100 °C for 30 min, placed back into the vacuum chamber of a probe station, and after a threeday evacuation at 2×10^{-6} Torr, measured again. The resulting temperature dependence of the resistivity shown in Figure 3b is very different from that of a freshly prepared MXene flake (Figure 3a) but looks very similar to the $\rho(T)$ plots that were previously reported for ${\rm Ti_3C_2T_{x^*}}^{9-11}$ First, the resistivity at room temperature increased from 1.77 $\mu\Omega$ m to 2.41 $\mu\Omega$ m, which is consistent with a partial oxidation of the MXene flake. Second, while the resistivity decreases when the temperature decreases from 290 to 125 K, showing a metallic behavior with $d\rho/dT > 0$, the sign of the slope reverses with further cooling to 9 K, showing a semiconductor-like behavior with $d\rho/dT$ < 0. The previously reported $\rho(T)$ dependences for $Ti_3C_2T_x$ also had resistivity minima, which were observed in the range from 90 to 250 K.9-11 Here, the resistivity minimum was found at 110 K, which is consistent with this temperature range.

It is expected that an oxidation of a MXene flake would increase the level of disorder, resulting in a stronger scattering. Therefore, we can employ Matthiessen's rule,³⁸ a simple phenomenological model that incorporates the effect of all types of scatterers on the transport properties of metals, and add a logarithmic term to eq 2, resulting in the following formula:

$$\rho(T) = \rho_0 + \rho_0 A \left(\frac{T}{\theta_{BG}}\right)^n \int_0^{\theta_{BG}/T} \frac{x^n}{(e^x - 1)(1 - e^{-x})} dx + \rho_0 B \ln(T)$$
(3)

where B is a constant related to scattering at low temperatures. The resulting fit for the oxidized monolayer $Ti_3C_2T_x$ device $(R^2 = 0.9979)$ is shown by the dashed gray line in Figure 3b. There are three corrections that exhibit the logarithmic behavior in 2D systems: the weak localization (WL), the electron–electron interaction (EEI) in a disordered system, and the Kondo effect. Therefore, it is difficult to identify the exact origin of the logarithmic temperature dependence of the resistivity at low temperatures without additional experiments. Similar behavior of the temperature-dependent resistivity in $Ti_3C_2T_x$ films was previously attributed to the WL effect.

While a partial oxidation of $Ti_3C_2T_r$ flakes is experimentally shown here to result in an emergence of a low-temperature logarithmic tail with $d\rho/dT < 0$, other kinds of MXene treatment resulting in an increased scattering should produce a similar effect. For example, Halim and co-workers investigated films of percolating Ti₃C₂T_x flakes and observed that this lowtemperature logarithmic tail increases upon intercalation of the films with NH₃ and NH₄⁺, compared to the nonintercalated films. In any case, the results of this work demonstrate that $Ti_3C_2T_x$ is intrinsically metallic with $d\rho/dT > 0$ in the entire 10-300 K temperature range, while the emergence of this lowtemperature logarithmic tail with $d\rho/dT < 0$ is an indication of extrinsic factors, such as oxidation or, possibly, adsorption/ intercalation. Since the $\rho(T)$ curves are sensitive to the disorder in Ti₃C₂T_{xy} these results suggest that temperaturedependent resistivity data could be used to assess the quality of a MXene material. A $\rho(T)$ dependence with $d\rho/dT > 0$ in a wide temperature range could suggest a high quality of a $Ti_3C_2T_x$ MXene, while a curve with a minimum would indicate a low-temperature electron scattering and invite additional investigations into its origin.

In addition to the studies on ${\rm Ti_3C_2T_x}$ monolayers, we also investigated devices based on multilayer ${\rm Ti_3C_2T_x}$ flakes; a representative example is shown in the SEM image in the inset in Figure 3c. The thickness of the flake was 10 nm, as measured by AFM. Based on our previous study of the correlation between the AFM thickness and the number of layers in multilayer ${\rm Ti_3C_2T_x}^3$ this flake contained eight monolayers. This flake was from the same batch of MXene as the monolayer ${\rm Ti_3C_2T_x}$ shown in Figure 3a,b. The two flakes were simultaneously deposited on a ${\rm Si/SiO_2}$ substrate and underwent the same treatment during the device fabrication and annealing on a hot plate, offering a direct comparison between the electronic properties of the corresponding monolayer and multilayer ${\rm Ti_3C_2T_x}$ devices.

The resistivity of the as-prepared multilayer MXene flake increases with temperature in the entire range from 9 to 300 K, as shown in Figure 3c. The $\rho(T)$ dependence shows metallic behavior and can also be accurately fitted with eq 2. The room-

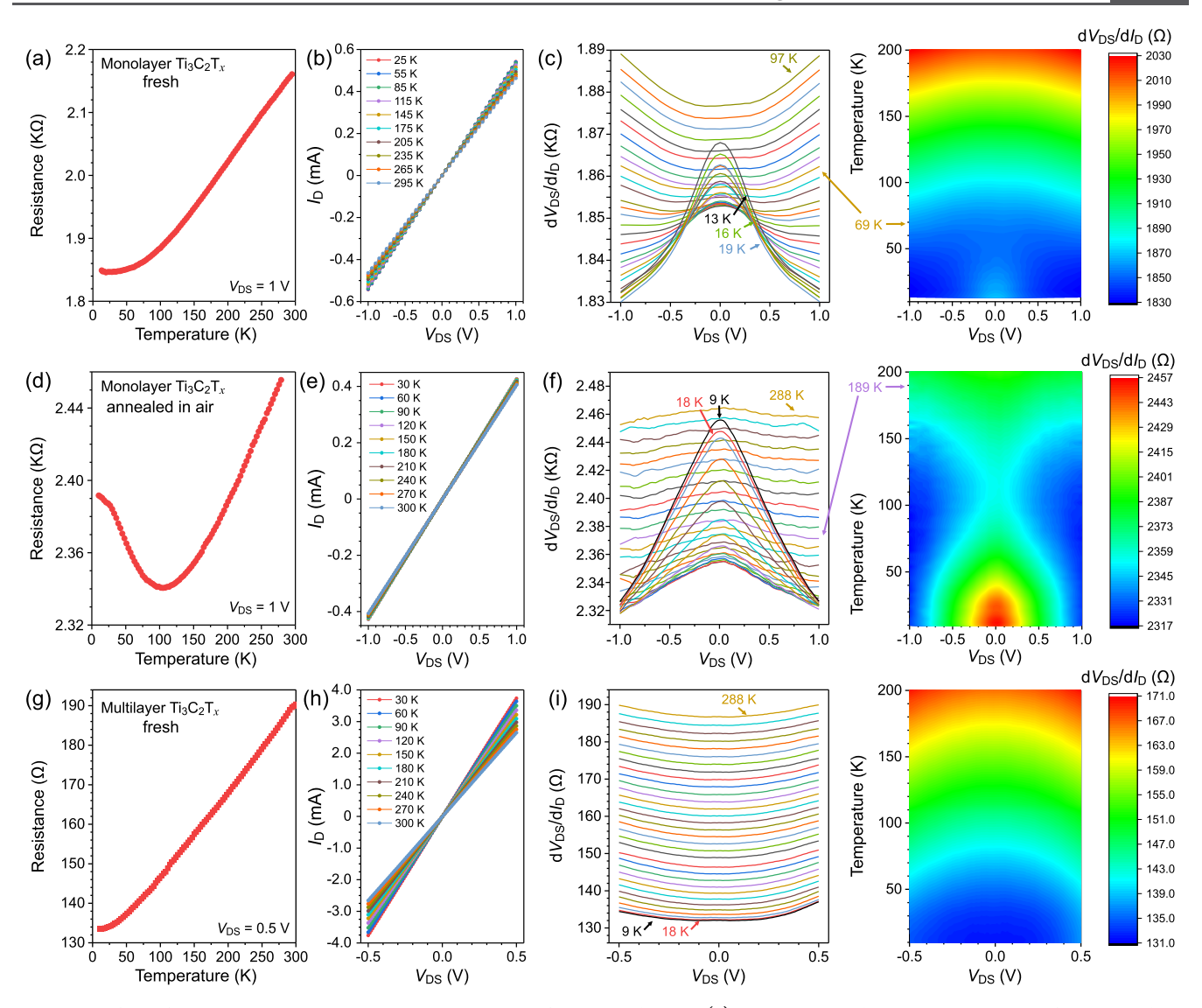


Figure 4. Effect of temperature on the electronic properties of $Ti_3C_2T_x$ devices. (a) Temperature-dependent resistance of the monolayer $Ti_3C_2T_x$ device shown in Figure 2b. (b) I_D-V_{DS} curves for the same device at selected temperatures. (c) Left: dV_{DS}/dI_D-V_{DS} curves for the same device at selected temperatures with the step of 3 K. Right: dV_{DS}/dI_D heat map for the temperatures from 13 to 200 K. (d) Temperature-dependent resistance of the partially oxidized monolayer $Ti_3C_2T_x$ device shown in Figure 3a. (e) I_D-V_{DS} curves for the same device at selected temperatures with the step of 9 K. Right: dV_{DS}/dI_D heat map for the temperatures from 10 to 200 K. (g) Temperature-dependent resistance of the as-prepared multilayer $Ti_3C_2T_x$ device shown in Figure 3c. (h) I_D-V_{DS} curves for the same device at selected temperatures. (i) Left: dV_{DS}/dI_D-V_{DS} curves for the same device at selected temperatures with the step of 9 K. Right: dV_{DS}/dI_D heat map for the temperatures from 10 to 200 K.

temperature sheet resistance for the film is $\rho_{\blacksquare} = 233 \ \Omega \ \Box^{-1}$, and accounting for the flake thickness of 8 monolayers, the conductivity is $\sigma = 5480 \ \text{S} \ \text{cm}^{-1}$, which is very close to the value for the monolayer flake in Figure 3a. This result indicates that the as-prepared monolayer and multilayer $\text{Ti}_3\text{C}_2\text{T}_x$ flakes were of similar quality.

The temperature dependence of the resistivity of the multilayer ${\rm Ti_3C_2T_x}$ flake after annealing in air is shown in Figure 3d. Unlike the monolayer device (Figure 3b), there is almost no change in the shape of the $\rho(T)$ curve after the treatment; compare Figures 3c and 3d. The room-temperature resistivity remains the same, 1.83 $\mu\Omega$ m, the resistivity increases with temperature in the entire range from 9 to 300 K, and the curve can be fitted with the same equation (eq 2). There is a small drop in the low-temperature resistance that may be attributed to improved electrical contacts between the

flake and the electrodes upon annealing, which would manifest stronger at low temperatures than at high temperatures. A comparison of the results of oxidation of monolayer (Figure 3a,b) and multilayer (Figure 3c,d) ${\rm Ti_3C_2T_x}$ flakes suggests that the outer layers of a multilayer flake protect the core layers from the environment, making thicker flakes more stable against oxidation. This result further suggests that multilayer MXene flakes may be beneficial for certain applications, particularly if the quality of the material and its environmental stability are important.

Additional insights into the low-temperature semiconductor-like behavior of MXene flakes, even at small levels of structural degradation, can be gained from temperature-dependent $I_{\rm D}-V_{\rm DS}$ curves, as summarized in Figure 4. We found that in the semiconductor-like regime (d $\rho/{\rm d}T<0$) at low temperatures, the partially oxidized MXene samples demonstrate nonlinear

 $I_{\mathrm{D}} - V_{\mathrm{DS}}$ curves, likely due to deteriorated contacts with the metallic electrodes of the devices, while the curves become linear at higher temperatures where $d\rho/dT > 0$. To illustrate this effect, we compare three different samples: a fresh monolayer (Figure 4a-c; the device shown in Figure 2b), a monolayer annealed in air (Figure 4d-f; the device shown in Figure 3a), and a fresh multilayer $Ti_3C_2T_r$ flake (Figure 4g-i; the device shown in Figure 3c). Figures 4a, 4d, and 4g show temperature-dependent resistivity plots for the respective devices, while Figures 4b, 4e, and 4h show the corresponding $I_{\mathrm{D}}{-}V_{\mathrm{DS}}$ curves recorded at different temperatures. These curves generally look linear, but subtle nonlinearities can be revealed if the data are presented in a differential form in the dV_{DS}/dI_D-V_{DS} coordinates. The corresponding dV_{DS}/dI_D-V_{DS} curves at different temperatures for all three devices are shown in the left panels in Figures 4c, 4f, and 4i, while the right panels show the same data as heat maps. The greater the dependence of dV_{DS}/dI_{D} on V_{DS} at a certain temperature, the more nonlinear the corresponding I_D – V_{DS} curve is, and vice versa. For the multilayer $Ti_3C_2T_x$ flake, which is resistant to degradation, the dV_{DS}/dI_D-V_{DS} curves are very consistent in the entire temperature range from 9 to 288 K (Figure 4i), which agrees well with the monotonous metallic $(d\rho/dT > 0)$ temperature dependence of its resistance (Figure 4g). A metallic multilayer Ti₃C₂T_x flake forms a good Ohmic contact with Ti/Au electrodes in this entire temperature range, which translates into linear I_D - V_{DS} curves (Figure 4h). The slight nonlinearity in the $I_{\rm D}{-}V_{\rm DS}$ curves in Figure 4h at higher voltages can be explained by the Joule heating of Ti₃C₂T_x MXene.

In contrast to the results obtained on degradation-resistant multilayer MXene flakes, $Ti_3C_2T_x$ monolayers show a much more pronounced nonlinear behavior at low temperatures. For the monolayer $Ti_3C_2T_x$ device that was annealed in air (Figure 4f), the $dV_{\rm DS}/dI_{\rm D}-V_{\rm DS}$ curves at low temperatures show a very pronounced maximum at $V_{\rm DS}$ = 0 that was not observed for the multilayer flake (Figure 4i). This maximum indicates the nonlinearity in the corresponding I_D-V_{DS} curves at low temperatures for the partially oxidized $Ti_3C_2T_x$ monolayer in a semiconductor-like regime (d $\rho/{\rm d}T$ < 0). The ${\rm d}V_{\rm DS}/{\rm d}I_{\rm D}$ maximum gradually decreases with increasing temperature, as the material transitions to the metallic regime with $d\rho/dT > 0$, and becomes barely visible around 190 K (Figure 4f), when the corresponding $\rho(T)$ dependence becomes completely linear. Similarly, the dV_{DS}/dI_D-V_{DS} curves can reveal some nonlinearity in the $I_{\rm D} - V_{\rm DS}$ curves for the fresh ${\rm Ti_3C_2T_x}$ monolayer (Figure 4c), despite the fact that the entire $\rho(T)$ dependence has $d\rho/dT > 0$ and can be fitted with eq 2. This nonlinearity completely disappears around 70 K and corresponds to the plateauing region of the $\rho(T)$ dependence at low temperatures (Figure 4a). Overall, the results in Figure 4 demonstrate that the temperature-dependent $dV_{DS}/dI_{D}-V_{DS}$ plots for MXene flakes correlate with their $\rho(T)$ dependences and can be used for revealing their semiconductor-like and metallic regimes. These data also suggest that despite our best efforts to produce high-quality monolayer Ti₃C₂T_x flakes and minimize their oxidation during the device fabrication, they still showed some nonlinear $I_D - V_{DS}$ behavior at low temperatures.

In summary, we fabricated electronic devices based on individual high-quality $\mathrm{Ti_3C_2T_x}$ flakes and performed their temperature-dependent resistivity measurements in the range from 10 to 300 K. Particular attention was paid to minimizing the exposure of $\mathrm{Ti_3C_2T_x}$ to air during the solution storage and

device fabrication to ensure the high quality of the flakes that were used for electrical measurements. These measurements revealed that the resistivity of flakes increases with temperature in the entire 10–300 K range, and the resulting $\rho(T)$ dependences can be accurately fitted by the Bloch-Grüneisen formula for the temperature dependence of the resistivity of metals, confirming the metallic nature of $Ti_3C_2T_r$. We also demonstrate that an oxidation of a $Ti_3C_2T_x$ monolayer transforms a monotonically increasing $\rho(T)$ curve into a dependence with a minimum that looks similar to the previously reported results. 9-11 The emerging low-temperature tail with a semiconductor-like $d\rho/dT < 0$ behavior can be explained by the stronger electron scattering in a partially oxidized MXene due to an increased level of disorder, and the resulting $\rho(T)$ curves can be accurately fitted using Matthiessen's rule, which incorporates the effect of all types of scatterers on the transport properties of metals.

Many applications of $Ti_3C_2T_x$ MXene in energy storage, 40 electromagnetic interference shielding, 41 gas sensing, 7 transparent conductive coatings, 8 electrical interconnects, 3 printed electronics, 42 and other areas exploit the metallic conductivity of the material, which makes the experimental verification of the metallic nature of $Ti_3C_2T_x$ ($d\rho/dT > 0$) important in a broad context. Our experiments also provide insights into the origin of the emergence of a low-temperature tail with $d\rho/dT$ < 0. More specifically, the low-temperature $d\rho/dT < 0$ tail indicates the electron scattering in a material, which may originate from the oxidation of MXene or, as was shown for percolating films of $Ti_3C_2T_x$ flakes, an intercalation into a film. Thus, since the $\rho(T)$ curves are sensitive to the disorder in Ti₃C₂T_x, these results suggest that temperature-dependent resistivity data could be used to assess the quality of a MXene material. A $\rho(T)$ dependence with $d\rho/dT > 0$ in a wide temperature range would be an indication of a high-quality $Ti_3C_2T_x$ MXene, while a curve with a minimum would suggest a low-temperature electron scattering and invite additional investigations into its origin.

Finally, we demonstrate that multilayer ${\rm Ti_3C_2T_x}$ flakes retain their purely metallic ${\rm d}\rho/{\rm d}T>0$ behavior even after oxidation in air, suggesting that the outer layers of multilayer flakes effectively protect the core layers from the environment. This result suggests that certain applications may benefit from the use of multilayer MXene flakes because of their improved environmental stability.

■ EXPERIMENTAL SECTION

Synthesis of Ti₃C₂T_x MXene. Ti (99%, 300 mesh), Al (99%, 300 mesh), and TiC (99.9%, 300 mesh) were purchased from Alfa Aesar. HCl was purchased from VWR, and LiF was purchased from Spectrum Chemical. All chemicals were used as received. Ti₃AlC₂ MAX phase was synthesized using the 2:2:1 molar ratio of TiC:Al:Ti. All precursors were mixed using a pestle and mortar, pressed into a pellet at 3500 psi, and annealed at 1450 °C for 8 h under a flow of argon (300 sccm). After the synthesis, the Ti₃AlC₂ MAX phase was crushed and sieved to collect uniformly sized particles; see Figure S1a in the Supporting Information.

 ${
m Ti}_3{
m C}_2{
m T}_x$ MXene was synthesized using the MILD method. ¹³ In brief, the MAX phase (500 mg, particle size below 38 $\mu{
m m}$) was slowly dispersed in 10 mL of HCl (9 M) containing LiF (800 mg) and stirred for 24 h (600 rpm, 25 °C). The sample was then washed and centrifuged until pH 6 was reached and then delaminated into flakes by mild shaking for 15 min.

During the washing and delamination steps, the sample was handled very gently to avoid flake tearing. ^{21,43}

Materials Characterization. For TEM characterization, Ti₃C₂T_x flakes were imaged using a FEI Tecnai Osiris transmission electron microscope equipped with a HAADF detector and an X-FEG high brightness Schottky field emission gun at the accelerating voltage of 200 kV. A sample of $Ti_3C_2T_x$ MXene was dispersed in an aqueous ethanol solution, deposited on a lacey carbon-coated Cu TEM grid, dried in air, and loaded into the instrument. SEM was performed using a Zeiss Supra 40 field-emission scanning electron microscope at the accelerating voltage of 5 kV. XRD patterns of Ti₃AlC₂ and Ti₃C₂T_r powders were collected by using a PANalytical Empyrean diffractometer in the Bragg-Brentano configuration operated at 45 kV and 40 mA with Ni-filtered Cu K α radiation. Quantitative Rietveld refinement of the powder XRD patterns was performed using JANA2006 software, 44 employing internal tables for X-ray atomic form factors. The chemical analysis of the samples by XPS was carried out using a Thermo Scientific K-alpha X-ray photoelectron spectrometer with monochromated Al K α (1486.6 eV) radiation and a low-energy electron flood gun for charge neutralization. The high-resolution Ti2p spectrum was recorded by using a pass energy of 20 eV and a 0.1 eV step. AFM was performed using a Bruker Dimension Icon atomic force microscope operated in PeakForce Tapping mode.

Device Fabrication and Electrical Measurements. A Zeiss Supra 40 field-emission scanning electron microscope and a Raith pattern generator were used for EBL to pattern electrodes on ${\rm Ti_3C_2T_x}$ flakes. An AJA electron beam evaporation system at the base pressure of ${\sim}8\times10^{-9}$ Torr was used to deposit Ti/Au contacts. The ${\rm Ti_3C_2T_x}$ devices were measured in a Lake Shore CRX-4K cryogenic probe station at a base pressure of about 2×10^{-6} Torr. After the evacuation, the devices were stored in vacuum for at least 2 days before the measurements to minimize the effect of surface adsorbates on the electronic characteristics. The electrical measurements were performed by using an Agilent 4155B semiconductor parameter analyzer that was operated using a National Instruments LabView code.

ASSOCIATED CONTENT

Supporting Information

The Supporting Information is available free of charge at https://pubs.acs.org/doi/10.1021/acsmaterialslett.3c01234.

SEM images of $\mathrm{Ti_3AlC_2}$ particles and $\mathrm{Ti_3C_2T_x}$ flakes (Figure S1); survey and Al2p XPS spectra of $\mathrm{Ti_3C_2T_x}$ MXene (Figure S2); additional optical photographs of $\mathrm{Ti_3C_2T_x}$ flakes deposited on $\mathrm{Si/SiO_2}$ and the corresponding distributions of monolayer, bilayer, and multilayer flakes (Figure S3) (PDF)

AUTHOR INFORMATION

Corresponding Authors

Alexey Lipatov — Department of Chemistry, Biology & Health Sciences and Karen M. Swindler Department of Chemical and Biological Engineering, South Dakota School of Mines and Technology, Rapid City, South Dakota 57701, United States; Occid.org/0000-0001-5043-1616; Email: alexey.lipatov@sdsmt.edu

Alexander Sinitskii – Department of Chemistry, University of Nebraska—Lincoln, Lincoln, Nebraska 68588, United

States; Nebraska Center for Materials and Nanoscience, University of Nebraska—Lincoln, Lincoln, Nebraska 68588, United States; orcid.org/0000-0002-8688-3451; Email: sinitskii@unl.edu

Author

Saman Bagheri — Department of Chemistry, University of Nebraska—Lincoln, Lincoln, Nebraska 68588, United States; orcid.org/0000-0002-4206-3021

Complete contact information is available at: https://pubs.acs.org/10.1021/acsmaterialslett.3c01234

Author Contributions

A.L. and A.S. conceived the idea of this study. S.B. prepared MAX phase and MXene samples and performed XPS, XRD, AFM, SEM, and TEM characterizations. A.L. fabricated MXene devices, performed electrical measurements, and analyzed the experimental results. A.L. and A.S. wrote the manuscript.

Notes

The authors declare no competing financial interest.

ACKNOWLEDGMENTS

The work was supported by the National Science Foundation through awards OSI-2329159 (A.L.) and OIA-2044049 (A.S.). Some experiments were performed using the instrumentation at the UNL instrumentation facilities supported by the National Science Foundation (award ECCS-2025298), the Nebraska Research Initiative, and the Nebraska Center for Energy Sciences Research.

REFERENCES

- (1) Gogotsi, Y.; Anasori, B. The Rise of MXenes. ACS Nano 2019, 13, 8491-8494.
- (2) Vahidmohammadi, A.; Rosen, J.; Gogotsi, Y. The world of two-dimensional carbides and nitrides (MXenes). *Science* **2021**, *372*, No. eabf1581.
- (3) Lipatov, A.; Goad, A.; Loes, M. J.; Vorobeva, N. S.; Abourahma, J.; Gogotsi, Y.; Sinitskii, A. High electrical conductivity and breakdown current density of individual monolayer ${\rm Ti}_3{\rm C}_2{\rm T}_x$ MXene flakes. *Matter* **2021**, *4*, 1413–1427.
- (4) Xie, Y.; Kent, P. R. C. Hybrid density functional study of structural and electronic properties of functionalized $\mathrm{Ti}_{(n+1)}X_n$ (X = C, N) monolayers. *Phys. Rev. B* **2013**, *87*, No. 235441.
- (5) Liu, Y.; Xiao, H.; Goddard, W. A. Schottky-Barrier-Free Contacts with Two-Dimensional Semiconductors by Surface-Engineered MXenes. *J. Am. Chem. Soc.* **2016**, *138*, 15853–15856.
- (6) Hart, J. L.; Hantanasirisakul, K.; Lang, A. C.; Anasori, B.; Pinto, D.; Pivak, Y.; van Omme, J. T.; May, S. J.; Gogotsi, Y.; Taheri, M. L. Control of MXenes' electronic properties through termination and intercalation. *Nat. Commun.* **2019**, *10*, 522.
- (7) Kim, S. J.; Koh, H.-J.; Ren, C. E.; Kwon, O.; Maleski, K.; Cho, S.-Y.; Anasori, B.; Kim, C.-K.; Choi, Y.-K.; Kim, J.; Gogotsi, Y.; Jung, H.-T. Metallic ${\rm Ti}_3{\rm C}_2{\rm T}_{\rm x}$ MXene Gas Sensors with Ultrahigh Signal-to-Noise Ratio. *ACS Nano* **2018**, *12*, 986–993.
- (8) Guo, T.; Zhou, D.; Deng, S.; Jafarpour, M.; Avaro, J.; Neels, A.; Heier, J.; Zhang, C. Rational Design of $Ti_3C_2T_x$ MXene Inks for Conductive, Transparent Films. *ACS Nano* **2023**, *17*, 3737–3749.
- (9) Halim, J.; Lukatskaya, M. R.; Cook, K. M.; Lu, J.; Smith, C. R.; Näslund, L.-Å.; May, S. J.; Hultman, L.; Gogotsi, Y.; Eklund, P.; Barsoum, M. W. Transparent Conductive Two-Dimensional Titanium Carbide Epitaxial Thin Films. *Chem. Mater.* **2014**, *26*, 2374–2381.
- (10) Anasori, B.; Shi, C.; Moon, E. J.; Xie, Y.; Voigt, C. A.; Kent, P. R. C.; May, S. J.; Billinge, S. J. L.; Barsoum, M. W.; Gogotsi, Y. Control of electronic properties of 2D carbides (MXenes) by

- manipulating their transition metal layers. *Nanoscale Horizons* **2016**, *1*, 227–234.
- (11) Miranda, A.; Halim, J.; Barsoum, M. W.; Lorke, A. Electronic properties of freestanding $Ti_3C_2T_x$ MXene monolayers. *Appl. Phys. Lett.* **2016**, *108*, No. 033102.
- (12) Zhang, C. J.; Pinilla, S.; McEvoy, N.; Cullen, C. P.; Anasori, B.; Long, E.; Park, S.-H.; Seral-Ascaso, A.; Shmeliov, A.; Krishnan, D.; Morant, C.; Liu, X.; Duesberg, G. S.; Gogotsi, Y.; Nicolosi, V. Oxidation Stability of Colloidal Two-Dimensional Titanium Carbides (MXenes). *Chem. Mater.* **2017**, *29*, 4848–4856.
- (13) Lipatov, A.; Alhabeb, M.; Lukatskaya, M. R.; Boson, A.; Gogotsi, Y.; Sinitskii, A. Effect of Synthesis on Quality, Electronic Properties and Environmental Stability of Individual Monolayer Ti₃C₂ MXene Flakes. *Advanced Electronic Materials* **2016**, *2*, No. 1600255.
- (14) Deng, S.; Guo, T.; Nüesch, F.; Heier, J.; Zhang, C. Stable MXene Dough with Ultrahigh Solid Fraction and Excellent Redispersibility toward Efficient Solution Processing and Industrialization. *Advanced Science* **2023**, *10*, No. 2300660.
- (15) Pazniak, H.; Plugin, I. A.; Loes, M. J.; Inerbaev, T. M.; Burmistrov, I. N.; Gorshenkov, M.; Polcak, J.; Varezhnikov, A. S.; Sommer, M.; Kuznetsov, D. V.; Bruns, M.; Fedorov, F. S.; Vorobeva, N. S.; Sinitskii, A.; Sysoev, V. V. Partially Oxidized Ti₃C₂T_x MXenes for Fast and Selective Detection of Organic Vapors at Part-per-Million Concentrations. *ACS Applied Nano Materials* **2020**, *3*, 3195–3204.
- (16) Choi, J.; Kim, Y.-J.; Cho, S.-Y.; Park, K.; Kang, H.; Kim, S. J.; Jung, H.-T. In Situ Formation of Multiple Schottky Barriers in a Ti₃C₂ MXene Film and its Application in Highly Sensitive Gas Sensors. *Adv. Funct. Mater.* **2020**, *30*, No. 2003998.
- (17) Liu, S.; Wang, M.; Liu, G.; Wan, N.; Ge, C.; Hussain, S.; Meng, H.; Wang, M.; Qiao, G. Enhanced NO₂ gas-sensing performance of 2D Ti₃C₂/TiO₂ nanocomposites by in-situ formation of Schottky barrier. *Appl. Surf. Sci.* **2021**, *567*, No. 150747.
- (18) Zhou, Y.; Wang, Y.; Wang, Y.; Yu, H.; Zhang, R.; Li, J.; Zang, Z.; Li, X. MXene Ti₃C₂T_x-Derived Nitrogen-Functionalized Heterophase TiO₂ Homojunctions for Room-Temperature Trace Ammonia Gas Sensing. ACS Appl. Mater. Interfaces **2021**, 13, 56485–56497.
- (19) Loes, M. J.; Bagheri, S.; Vorobeva, N. S.; Abourahma, J.; Sinitskii, A. Synergistic Effect of TiS₃ and Ti₃C₂T_x MXene for Temperature-Tunable p-/n-Type Gas Sensing. ACS Applied Nano Materials **2023**, *6*, 9226–9235.
- (20) Alhabeb, M.; Maleski, K.; Anasori, B.; Lelyukh, P.; Clark, L.; Sin, S.; Gogotsi, Y. Guidelines for Synthesis and Processing of Two-Dimensional Titanium Carbide (Ti₃C₂T_x MXene). *Chem. Mater.* **2017**, 29, 7633–7644.
- (21) Shekhirev, M.; Busa, J.; Shuck, C. E.; Torres, A.; Bagheri, S.; Sinitskii, A.; Gogotsi, Y. Ultralarge Flakes of $Ti_3C_2T_x$ MXene via Soft Delamination. *ACS Nano* **2022**, *16*, 13695–13703.
- (22) Mathis, T. S.; Maleski, K.; Goad, A.; Sarycheva, A.; Anayee, M.; Foucher, A. C.; Hantanasirisakul, K.; Shuck, C. E.; Stach, E. A.; Gogotsi, Y. Modified MAX Phase Synthesis for Environmentally Stable and Highly Conductive Ti₃C₂ MXene. *ACS Nano* **2021**, *15*, 6420–6429.
- (23) Shuck, C. E.; Han, M.; Maleski, K.; Hantanasirisakul, K.; Kim, S. J.; Choi, J.; Reil, W. E. B.; Gogotsi, Y. Effect of Ti₃AlC₂ MAX Phase on Structure and Properties of Resultant Ti₃C₂T_x MXene. ACS Applied Nano Materials **2019**, *2*, 3368–3376.
- (24) Bagheri, S.; Lipatov, A.; Vorobeva, N. S.; Sinitskii, A. Interlayer Incorporation of A-Elements into MXenes Via Selective Etching of A' from $M_{n+1}A'_{1-x}A''_{x}C_{n}$ MAX Phases. ACS Nano 2023, 17, 18747–18757.
- (25) Vorobeva, N. S.; Bagheri, S.; Torres, A.; Sinitskii, A. Negative photoresponse in Ti₃C₂T_x MXene monolayers. *Nanophotonics* **2022**, *11*, 3953–3960.
- (26) Lipatov, A.; Lu, H.; Alhabeb, M.; Anasori, B.; Gruverman, A.; Gogotsi, Y.; Sinitskii, A. Elastic properties of 2D Ti₃C₂T_x MXene monolayers and bilayers. *Science Advances* **2018**, *4*, No. eaat0491.
- (27) Wang, X.; Shen, X.; Gao, Y.; Wang, Z.; Yu, R.; Chen, L. Atomic-Scale Recognition of Surface Structure and Intercalation Mechanism of Ti₃C₂X. *J. Am. Chem. Soc.* **2015**, *137*, 2715–2721.

- (28) Natu, V.; Benchakar, M.; Canaff, C.; Habrioux, A.; Célérier, S.; Barsoum, M. W. A critical analysis of the X-ray photoelectron spectra of Ti₃C₂T₂ MXenes. *Matter* **2021**, *4*, 1224–1251.
- (29) Halim, J.; Cook, K. M.; Naguib, M.; Eklund, P.; Gogotsi, Y.; Rosen, J.; Barsoum, M. W. X-ray photoelectron spectroscopy of select multi-layered transition metal carbides (MXenes). *Appl. Surf. Sci.* **2016**, 362, 406–417.
- (30) Barsoum, M. W.; Gogotsi, Y. Removing roadblocks and opening new opportunities for MXenes. *Ceram. Int.* **2023**, *49*, 24112–24122.
- (31) Kittel, C. Introduction to Solid State Physics, 8th ed.; Wiley, 2004.
- (32) Persson, I.; Näslund, L.-Å.; Halim, J.; Barsoum, M. W.; Darakchieva, V.; Palisaitis, J.; Rosen, J.; Persson, P. O. Å. On the organization and thermal behavior of functional groups on Ti₃C₂ MXene surfaces in vacuum. 2D Materials **2018**, 5, No. 015002.
- (33) Bilyk, T.; Benchakar, M.; Bugnet, M.; Loupias, L.; Chartier, P.; Pazniak, H.; David, M. L.; Habrioux, A.; Celerier, S.; Pacaud, J.; Mauchamp, V. Electronic Structure Sensitivity to Surface Disorder and Nanometer-Scale Impurity of 2D Titanium Carbide MXene Sheets as Revealed by Electron Energy-Loss Spectroscopy. *J. Phys. Chem. C* 2020, 124, 27071–27081.
- (34) Stormer, H. L.; Pfeiffer, L. N.; Baldwin, K. W.; West, K. W. Observation of a Bloch-Gruneisen regime in two-dimensional electron transport. *Phys. Rev. B* **1990**, *41*, 1278–1281.
- (35) Efetov, D. K.; Kim, P. Controlling Electron-Phonon Interactions in Graphene at Ultrahigh Carrier Densities. *Phys. Rev. Lett.* **2010**, *105*, No. 256805.
- (36) Chelikowsky, J. R.; Louie, S. G. Quantum theory of real materials; Kluwer Academic Publishers: Boston, 1996.
- (37) Michałowski, P. P.; Anayee, M.; Mathis, T. S.; Kozdra, S.; Wójcik, A.; Hantanasirisakul, K.; Jóźwik, I.; Piątkowska, A.; Możdżonek, M.; Malinowska, A.; Diduszko, R.; Wierzbicka, E.; Gogotsi, Y. Oxycarbide MXenes and MAX phases identification using monoatomic layer-by-layer analysis with ultralow-energy secondary-ion mass spectrometry. *Nat. Nanotechnol.* **2022**, *17*, 1192–1197.
- (38) Matthiessen, A. On the electric conducting power of the metals. *Philosophical Transactions of the Royal Society of London* **1858**, 148, 383–387
- (39) Jobst, J.; Kisslinger, F.; Weber, H. B. Detection of the Kondo effect in the resistivity of graphene: Artifacts and strategies. *Phys. Rev. B* **2013**, 88, No. 155412.
- (40) Ling, Z.; Ren, C. E.; Zhao, M.-Q.; Yang, J.; Giammarco, J. M.; Qiu, J.; Barsoum, M. W.; Gogotsi, Y. Flexible and conductive MXene films and nanocomposites with high capacitance. *Proc. Natl. Acad. Sci. U. S. A.* **2014**, *111*, 16676–16681.
- (41) Shahzad, F.; Alhabeb, M.; Hatter, C. B.; Anasori, B.; Man Hong, S.; Koo, C. M.; Gogotsi, Y. Electromagnetic interference shielding with 2D transition metal carbides (MXenes). *Science* **2016**, 353, 1137–1140.
- (42) Zhang, Y.-Z.; Wang, Y.; Jiang, Q.; El-Demellawi, J. K.; Kim, H.; Alshareef, H. N. MXene Printing and Patterned Coating for Device Applications. *Adv. Mater.* **2020**, *32*, No. 1908486.
- (43) Bagheri, S.; Abourahma, J.; Lu, H.; Vorobeva, N. S.; Luo, S.; Gruverman, A.; Sinitskii, A. High-yield fabrication of electromechanical devices based on suspended ${\rm Ti_3C_2T_x}$ MXene monolayers. *Nanoscale* **2023**, *15*, 1248–1259.
- (44) Petříček, V.; Dušek, M.; Palatinus, L. Crystallographic Computing System JANA2006: General features. *Z. Krist.-Cryst. Mater.* **2014**, 229, 345–352.
- (45) Sinitskii, A.; Dimiev, A.; Kosynkin, D. V.; Tour, J. M. Graphene Nanoribbon Devices Produced by Oxidative Unzipping of Carbon Nanotubes. *ACS Nano* **2010**, *4*, 5405–5413.